

Two-phase transport and the role of micro-porous layer in polymer electrolyte fuel cells

Ugur Pasaogullari, Chao-Yang Wang*

*Department of Mechanical and Nuclear Engineering, and Electrochemical Engine Center (ECEC),
The Pennsylvania State University, University Park, PA 16802, USA*

Received 8 March 2004; received in revised form 20 April 2004; accepted 20 April 2004

Available online 2 June 2004

Abstract

Two-phase transport of reactants and products constitutes an important limit in performance of polymer electrolyte fuel cells (PEFC). Particularly, at high current densities and/or low gas flow rates, product water condenses in open pores of the cathode gas diffusion layer (GDL) and limits the effective oxygen transport to the active catalyst sites. Furthermore, liquid water covers some of the active catalytic surface, rendering them inactive for electrochemical reaction. Traditionally, these two-phase transport processes in the GDL are modeled using so-called unsaturated flow theory (UFT), in which a uniform gas-phase pressure is assumed across the entire porous layer, thereby ignoring the gas-phase flow counter to capillarity-induced liquid motion. In this work, using multi-phase mixture (M^2) formalism, the constant gas pressure assumption is relaxed and the effects of counter gas-flow are studied and found to be a new oxygen transport mechanism. Further, we analyze the multi-layer diffusion media, composed of two or more layers of porous materials having different pore sizes and/or wetting characteristics. Particularly, the effects of porosity, thickness and wettability of a micro-porous layer (MPL) on the two-phase transport in PEFC are elucidated.

© 2004 Elsevier Ltd. All rights reserved.

Keywords: PEFC; Flooding; Two-phase transport; Micro-porous layer; Gas diffusion layer; Water management

1. Introduction

Polymer electrolyte fuel cells (PEFC) have been the center of attention for over a decade as a possible candidate for next-generation energy conversion, being versatile, highly efficient and environmentally friendly. In the past two decades, research has accelerated in order to successfully deploy this promising technology in daily life, particularly for terrestrial transportation to increase the overall energy conversion efficiency and reduce exhaust emissions of automobiles.

Due to its lower operating temperatures (~ 70 – 90 °C), PEFC is prone to gas-liquid two-phase formation, particularly under highly humidified or high current density conditions. When GDL and catalyst layer become saturated with water vapor, the product water starts to condense and block open pores, reducing the available paths for oxygen trans-

port. This phenomenon is termed “flooding” and becomes a major limiting factor of PEFC performance. Hence, it is critical to understand the two-phase flow and transport in PEFC, and a mathematical model is useful to improve this understanding.

Several studies on two-phase transport in PEFC have appeared [1–7]. While some studies incorporated the flooding effects as a lumped parameter into single-phase transport equation via a reduced effective diffusivity [1,2], others have modeled two-phase transport, but in the hydrophilic GDL [3–7]. Whereas these prior studies shed light on the effect of flooding on PEFC performance, investigation and analysis of two-phase transport in hydrophobic GDL have been lacking. Only until most recently, Nam and Kaviani [8] and Pasaogullari and Wang [9] proposed a theory describing liquid-water transport in hydrophobic GDL. A brief review of this subject was given most recently by Wang [10].

The objective of the present study is two-fold. The first goal is to introduce a one-dimensional analytical model of liquid-gas, two-phase transport, using the well-established

* Corresponding author. Tel.: +814-863-4762; fax: +814-863-4848.
E-mail address: cwx31@psu.edu (C.-Y. Wang).

multi-phase mixture (M^2) formulation [11], which allows modeling of co-existent two-phase and single-phase regions. Traditionally, unsaturated flow theory (UFT) has been followed in PEFC modeling [4,7,8], which has to assume a constant gas pressure across the GDL. We shall assess this assumption implicit to UFT by using the more complete M^2 model. The second objective is to investigate the effect of the micro-porous layer (MPL) on liquid-water transport across the cathode gas diffusion medium, which consists of the coarse GDL and thin and finer MPL. MPL is often placed between a coarse GDL and the catalyst layer and has vastly different micro-structural and wetting characteristics. We shall analyze the effect of MPL through a parametric study by varying the porous and wetting characteristics as well as relative thickness, in order to optimize the MPL properties.

2. Model development

The present analytical study focuses on two-phase transport taking place in the cathode due to the production of water in the cathode catalyst layer and the electro-osmotic drag of water across the membrane. Therefore, the problem domain under consideration is confined to the cathode GDL, where the major mass transport limitations occur. We also assume the catalyst layer to be infinitely thin and the oxygen reduction reaction (ORR) takes place at the interface of polymer electrolyte membrane (PEM) and GDL, in the case of a single-layer GDL. A schematic of the modeling domain is given in Fig. 1, along with the associated transport processes. In the case of two-layer gas diffusion medium, consisting of a coarse GDL and a finer MPL, the domain is extended to include the MPL which is sandwiched between PEM and GDL, and the ORR is assumed to take place at

the interface between MPL and PEM. The present model for the two-phase transport in GDL can be readily integrated into a full fuel cell model to investigate GDL–catalyst layer interactions, and water flow among the cathode gas diffusion medium, the membrane, and the anode GDL. Such an example was presented in [12].

2.1. Unsaturated flow theory (UTF)

Much of the prior fuel cell models treating two-phase transport in GDL have been using a theory known widely as unsaturated flow theory (UFT) in the larger community of two-phase flow through porous media [11]. UFT entails an essential assumption that the gas-phase pressure is constant across the porous medium; therefore the liquid-phase pressure simply becomes the negative of capillary pressure between gas and liquid phases; i.e.:

$$p_c = p_g - p_l \tag{1}$$

The liquid-phase flux is expressed by Darcy’s law using the relative permeability of individual phases.

$$\vec{u}_l = -\frac{Kk_{rl}}{\mu_l} \nabla p_l \tag{2}$$

where k_{rl} represents the relative permeability of liquid phase. In this work, we assume isotropic GDL with the relative permeability of each individual phase proportional to the cube of phase saturations, i.e.:

$$k_{rl} = s^3, \quad k_{rg} = (1 - s)^3 \tag{3}$$

Since UFT approximation involves the constant gas-phase pressure across the porous media, liquid pressure can be expressed as:

$$p_l = -p_c + p_g, \quad \nabla p_l = -\nabla p_c \tag{4}$$

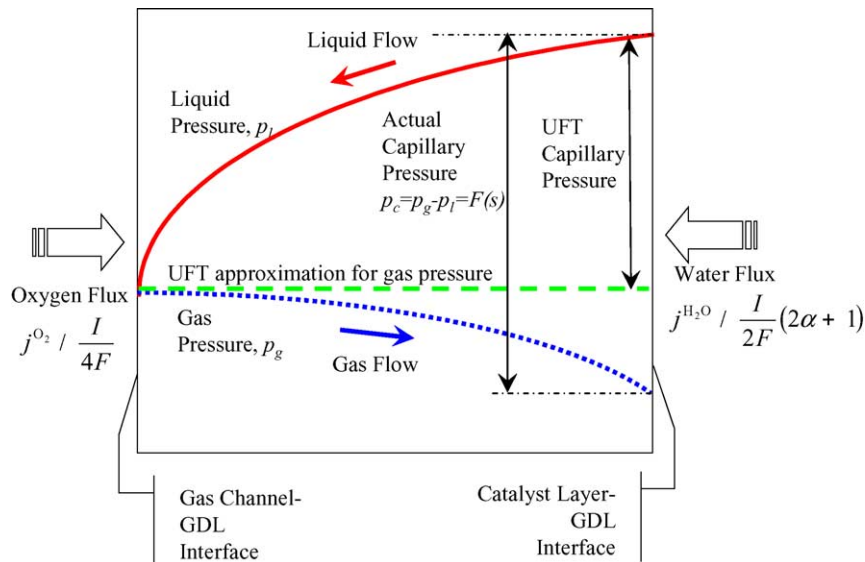


Fig. 1. Modeling domain and transport processes for a single layer GDL.

Then, the liquid velocity is given as:

$$\vec{u}_l = \frac{Kk_{rl}}{\mu_l} \nabla p_c \quad (5)$$

Capillary pressure between gas and liquid phases can be related to the phase saturations via [11]:

$$p_c = \sigma \cos(\theta_c) \left(\frac{\varepsilon}{K}\right)^{1/2} J(s) \quad (6)$$

where $J(s)$ is the Leverett function, and given by [9]:

$$J(s) = \begin{cases} 1.417(1-s) - 2.120(1-s)^2 + 1.263(1-s)^3, & \text{if } \theta_c < 90^\circ \\ 1.417s - 2.120s^2 + 1.263s^3, & \text{if } \theta_c > 90^\circ \end{cases} \quad (7)$$

Note that for a hydrophilic medium, the wetting phase is the liquid phase, therefore Leverett function is expressed in terms of gas-phase saturation, whereas in hydrophobic medium, the gas phase becomes the wetting phase and so the liquid-phase saturation is used. Contact angle, θ_c , of the GDL is dependent upon hydrophilic ($0^\circ < \theta_c < 90^\circ$) or hydrophobic ($90^\circ < \theta_c < 180^\circ$) nature of the GDL, and varies with the Teflon content. Here, the surface tension σ , for liquid-water-air system is taken as 0.0625 N/m. Combining Eq. (6) with Eq. (5), the liquid-water velocity is expressed in terms of liquid saturation such that:

$$\vec{u}_l = \frac{\sigma \cos(\theta_c)}{\mu_l} (\varepsilon K)^{1/2} k_{rl} \frac{dJ(s)}{ds} \nabla s \quad (8)$$

Then, a governing equation for liquid-water transport is obtained by combining the above relation of liquid-water velocity (Eq. (8)) with the liquid continuity equation, which is:

$$\frac{\partial(\varepsilon \rho_l s)}{\partial t} + \nabla(\rho_l \vec{u}_l) = 0 \quad (9)$$

In this work, due to the assumption of isothermal system, no condensation or evaporation takes place in the porous GDL. Note that also, since the water vapor concentration remains constant at the saturation value across the GDL, the gas-phase diffusion of water vanishes. Furthermore, the implicit assumption of constant gas-phase pressure in UFT model also leads to zero gas-phase velocity. Therefore, the only mode of water transport in the GDL is the capillary transport of liquid water. Here, the net water flux across the membrane from anode to cathode is assumed to be constant and characterized by a net water transport coefficient, α . Combining net water transport with water production, Eq. (9) is integrated over the GDL under steady-state, which yields to:

$$\rho_l \vec{u}_l = -\frac{I}{2F} (2\alpha + 1) M^{\text{H}_2\text{O}} \quad (10)$$

where the right-hand side represents the net water flux into GDL.

Inserting Eq. (10) into (8) yields:

$$-D_c \nabla s = -\frac{I}{2F} (2\alpha + 1) M^{\text{H}_2\text{O}} \quad (11)$$

The general form of the above equation is usually known as *Richards equation* and is traditionally solved similar to a diffusion equation. Here, D_c is:

$$D_c = -\frac{\sigma \cos(\theta_c)}{\nu_l} (\varepsilon K)^{1/2} k_{rl} \frac{dJ(s)}{ds} \quad (12)$$

Eq. (11) is a first-order ordinary differential equation, which requires one boundary condition. In general, this boundary condition is governed by the two-phase flow in the channel and liquid droplet size and distribution on the GDL

surface, however in this work, the gas channel is assumed to be free of liquid water and hence, the liquid saturation at the channel-GDL interface is assumed to be zero. This condition of zero surface coverage by liquid water is quite valid for carbon cloth GDL and holds true for carbon paper GDL under large air stoichiometry.

2.2. M^2 model

The multi-phase mixture model (M^2) is an exact re-formulation of classical two-fluid, two-phase model in a single equation. The main difference from UFT is that it does not require the approximation of constant gas-phase pressure. Another salient feature of M^2 is that it can be conveniently used in a problem domain where single- and double-phase zones co-exist. In the classical two-fluid models, the interface between single- and double-phase zones has to be tracked explicitly, which substantially increases the numerical complexity.

Mass conservation for the two-phase mixture as given by M^2 model is:

$$\frac{\partial(\varepsilon \rho)}{\partial t} + \nabla(\rho \vec{u}) = 0 \quad (13)$$

Similarly to UFT model, the above equation implies no phase change in the isothermal, two-phase system across the GDL. In the above, \vec{u} is the superficial two-phase mixture velocity vector. Here, the density of the two-phase mixture is defined as [11]:

$$\rho = \rho_l s + \rho_g (1 - s) \quad (14)$$

When the continuity equation for the two-phase mixture (Eq. (13)) is integrated over the GDL under steady-state, one has:

$$\rho u = -\frac{I}{2F} (2\alpha + 1) M^{\text{H}_2\text{O}} + \frac{I}{4F} M^{\text{O}_2} \quad (15)$$

where the right-hand side is net mass flux from GDL through both gas and liquid phases. Here, the first term in the right-hand side represents the net water flux into the GDL at the GDL/CL interface, while the second term is the net oxygen flux out of the GDL. The species conservation equation of M^2 model, written in terms of molar

concentration, is [12]:

$$\varepsilon \frac{\partial(C^i)}{\partial t} + \nabla(\gamma_c^i \vec{u} C^i) = \nabla[\varepsilon D_g^{i,\text{eff}}(1-s) \nabla C_g^i] - \nabla \left[\left(\frac{mf_1^i}{M^i} - \frac{C_g^i}{\rho_g} \right) \vec{j}_1 \right] \quad (16)$$

Note that, the gas and liquid phases have different velocities, therefore, the convective transport of the total two-phase mixture needs to be corrected via an advection correction factor, γ_c , i.e. [12]:

$$\gamma_c = \begin{cases} \frac{\rho}{C_{\text{H}_2\text{O}}} \left(\frac{\lambda_1}{M_{\text{H}_2\text{O}}} + \lambda_g \frac{C_{\text{H}_2\text{O}}}{\rho_g} \right) & \text{for water} \\ \frac{\rho \lambda_g}{\rho_g(1-s)} & \text{for other species} \end{cases} \quad (17)$$

Here, the effective diffusivity of gas phase, $D_g^{i,\text{eff}}$ is modified according to Bruggeman correlation [13], such as:

$$D_g^{i,\text{eff}} = [\varepsilon(1-s)]^\tau D_g^i \quad (18)$$

The significant departure of Eq. (16) from a single-phase species conservation equation is the last term on the right-hand side, which describes the transport of species via capillarity-induced motion (i.e. capillary transport). Note that, the capillary transport term in this equation, contrary to the UFT approach, also accounts for the gas flow counter to the capillary-driven liquid flow. For details of M^2 model development and how gas-phase pressure and counter-gas flow are incorporated into the model formulation, the reader is referred to [11]. Here, in the absence of gravity, liquid flux, \vec{j}_1 , is given by [11]:

$$\vec{j}_1 = \frac{\lambda_1 \lambda_g}{\nu} K \nabla p_c \quad (19)$$

where λ_1 and λ_g are the relative mobilities of liquid- and gas-phases, respectively [11]:

$$\lambda_1(s) = \frac{k_{rl}/v_l}{k_{rl}/v_l + k_{rg}/v_g} \quad \lambda_g(s) = 1 - \lambda_1(s) \quad (20)$$

If GDL is isothermal and saturated with water vapor, the water vapor concentration is uniform, thus the gas-phase diffusion vanishes. Moreover, in PEFC, only water is present in liquid phase, hence the mass fraction of water in liquid phase, $mf_1^{\text{H}_2\text{O}}$ is uniformly unity. Therefore, under steady state, Eq. (16) can be rewritten for water species as:

$$\nabla(\gamma_c \vec{u} C_{\text{H}_2\text{O}}) + \nabla \left[\left(\frac{1}{M_{\text{H}_2\text{O}}} - \frac{C_{\text{sat}}^{\text{H}_2\text{O}}}{\rho_g} \right) \vec{j}_1 \right] = 0 \quad (21)$$

Integration of the above equation over the GDL thickness yields:

$$\gamma_c u C_{\text{H}_2\text{O}} + \left(\frac{1}{M_{\text{H}_2\text{O}}} - \frac{C_{\text{sat}}^{\text{H}_2\text{O}}}{\rho_g} \right) j_1 = -\frac{I}{2F} (2\alpha + 1) \quad (22)$$

where the right-hand side represents the net molar water flux into GDL from the catalyst layer, I being the local

current density and α the net water transfer coefficient, which combines electro-osmotic drag and backward (i.e. cathode to anode) diffusion in the membrane. In this work, α is assumed to be equal to 0.5.

The total water concentration is expressed in terms of liquid saturation as [12]:

$$C_{\text{H}_2\text{O}} = \frac{\rho_l s}{M_{\text{H}_2\text{O}}} + C_{\text{sat}}^{\text{H}_2\text{O}} (1-s) \quad (23)$$

Using this relation, Eq. (22) can be rewritten using liquid saturation as the primary variable. Inserting the mixture velocity from Eq. (15), mixture density from Eq. (14), advection correction factor from Eq. (17) and liquid flux from Eq. (19) into Eq. (22), a governing equation of liquid saturation is written as:

$$\begin{aligned} & \frac{\gamma_c}{\rho_g(1-s) + \rho_l s} \left(-\frac{I}{2F} (2\alpha + 1) M_{\text{H}_2\text{O}} + \frac{I}{2F} M_{\text{O}_2} \right) \\ & \times \left(\frac{\rho_l s}{M_{\text{H}_2\text{O}}} + C_{\text{sat}}^{\text{H}_2\text{O}} (1-s) \right) + \left(\frac{1}{M_{\text{H}_2\text{O}}} - \frac{C_{\text{sat}}^{\text{H}_2\text{O}}}{\rho_g} \right) \\ & \times \left(\frac{\lambda_1 \lambda_g}{\nu} K \sigma \cos(\theta_c) \left(\frac{\varepsilon}{K} \right)^{1/2} \frac{dJ(s)}{ds} \nabla s \right) \\ & = -\frac{I}{2F} (2\alpha + 1) \end{aligned} \quad (24)$$

This equation is a non-linear first-order ordinary differential equation for the unknown liquid saturation, s , which requires one Dirichlet-type boundary condition. The same boundary condition described for UFT, which assumes zero liquid saturation at the GDL–channel interface is also used for this equation.

Once the liquid saturation profile is obtained from Eq. (24) and the mixture velocity, u calculated from Eq. (15), the individual velocities of liquid and gas phases can be calculated as follows:

$$\rho_l \vec{u}_l = \vec{j}_1 + \lambda_1 \rho \vec{u} \quad (25)$$

$$\rho_g \vec{u}_g = -\vec{j}_1 + \lambda_g \rho \vec{u} \quad (26)$$

The individual phase pressures are then obtained from Darcy's law, e.g.:

$$\nabla p_k = \frac{\mu_k}{K k_{rk}} \vec{u}_k \quad (27)$$

2.3. Multi-layer diffusion media

It is been widely recognized that liquid-water transport in the porous cathode can be improved by utilizing composite porous structures, consisting of multiple layers of different micro-porous and wetting characteristics. Kong et al. [14] found that introducing large pores in GDL increase cell performance by accumulating liquid water in the larger pores and providing a better path for reactant transport. Advantages of placing a thin micro-layer between PEM and GDL were also experimentally demonstrated by Qi and Kaufman

[15]. In this work, we analyze the multi-layer diffusion media on two-phase transport in the cathode of PEFC, which consists of a coarse GDL and a finer micro-porous layer (MPL), both of which are hydrophobic. The liquid-water transport in MPL is also governed by capillary action; therefore, the gas and liquid pressures across the interface of these two layers are continuous. That is,

$$p_c^{\text{GDL}} \Big|_{\text{GDL-MPL int}} = p_c^{\text{MPL}} \Big|_{\text{GDL-MPL int}} \quad (28)$$

However, the different properties of two layers cause a discontinuity in the liquid saturation across the interface of these two layers and this discontinuity is utilized as an advantage to decrease the liquid saturation in the MPL. Using Eq. (6), the continuity of phase pressures at the interface of two layers is expressed as:

$$\begin{aligned} \cos(\theta_c^{\text{GDL}}) \left(\frac{\varepsilon^{\text{GDL}}}{K^{\text{GDL}}} \right)^{1/2} J(s_{\text{int}}^{\text{GDL}}) \\ = \cos(\theta_c^{\text{MPL}}) \left(\frac{\varepsilon^{\text{MPL}}}{K^{\text{MPL}}} \right)^{1/2} J(s_{\text{int}}^{\text{MPL}}) \end{aligned} \quad (29)$$

Since the primary variable of liquid-water transport equation (i.e. liquid saturation, s) is discontinuous in this model, the following two steps are followed for numerical solution: first, the liquid saturation in GDL is solved using Eq. (24), utilizing the GDL–channel interface boundary condition. Once the liquid saturation of the GDL at the GDL–MPL interface is known from the GDL solution, the liquid saturation of MPL at the interface can be calculated using Eq. (29), and solution of Eq. (24) proceeds similarly in MPL.

2.4. Oxygen transport

The gas-phase flow counter to the capillarity-induced liquid motion provides an additional mode of oxygen transport, which has been generally overlooked in previous studies. Including this additional mode, the oxygen species conservation provided by M^2 formulation is:

$$\begin{aligned} \varepsilon \frac{\partial(C^{O_2})}{\partial t} + \nabla(\gamma_c \vec{u} C^{O_2}) = \nabla[\varepsilon D_g^{O_2, \text{eff}} (1-s) \nabla C^{O_2}] \\ + \nabla \left(\frac{C^{O_2}}{\rho_g} \vec{j}_l \right) \end{aligned} \quad (30)$$

The first term on the left-hand side is the transient term, describing the accumulation of oxygen species, whereas the first term on the right-hand side describes the diffusive flux. Note that the diffusion coefficient of oxygen is a function of liquid saturation, since the available open pore path for oxygen diffusion decreases with increasing liquid fraction. The most notably different part of this equation from earlier works is the convective component of the equation, which is composed of modified advective term (second term on the left-hand side) and capillary term (last term on the right-hand

side). Integrating Eq. (30) across the GDL in steady-state yields:

$$\left(\gamma_c \vec{u} - \frac{\vec{j}_l}{\rho_g} \right) C^{O_2} - \varepsilon D_g^{O_2, \text{eff}} (1-s) \nabla C^{O_2} = \frac{I}{4F} \quad (31)$$

where the right-hand side represents the net oxygen flux across the GDL, which is obtained from the Faraday’s law based on the local current density. Similar to water species conservation equation, this equation also requires a Dirichlet-type boundary condition. In this work, this boundary condition is obtained from the convective mass transport analysis of gas channel, using the heat and mass transfer analogy [9]. The oxygen concentration at the GDL surface is calculated by:

$$h_m (C_{\text{GDL-channel int}}^{O_2} - C_{\text{channel, } \infty}^{O_2}) = -\frac{I}{4F} \quad (32)$$

where the convective mass transfer coefficient, h_m , is given by:

$$h_m = \frac{Sh D^{O_2}}{D_h} \quad (33)$$

and using the heat and mass transfer analogy, Sherwood number is calculated from:

$$Sh = Nu \frac{Pr}{Sc} \quad (34)$$

3. Results and discussion

3.1. Comparison of UFT and M^2 model predictions

The two approaches for modeling two-phase transport in PEFC, namely UFT and M^2 , are compared in the 1D single-layer domain shown in Fig. 1. The governing equations, Eqs. (11) and (24), respectively, are solved numerically by using a Runge–Kutta method with adaptive step size. The model input parameters and physical properties are summarized in Table 1.

In Fig. 2, the liquid saturation profiles predicted by the two models are compared. Here, the local current density is taken to be 2 A/cm^2 . It is clearly seen that the UFT model under-predicts the liquid saturation in the GDL, due to the uniform gas-phase pressure assumption. In the M^2 model prediction, the counter-gas flow, which causes the gas-phase pressure to decrease from the channel to the catalyst layer is also accounted for. Therefore, under the same capillary pressure, the liquid pressure becomes smaller due to the smaller gas pressure ($p_l = p_g - p_c$). In order to maintain the same liquid flux, the capillary pressure, which is a function of liquid saturation, has to be higher, thus requiring a higher liquid saturation gradient across the GDL. Furthermore, the counter-gas flow also carries saturated water vapor from the channel toward the catalyst layer, which further increases the amount of liquid water to be transported away from the cat-

Table 1
Physical properties and parameters

Property	
Total cathode gas diffuser thickness (μm)	300
GDL contact angle, θ_c ($^\circ$)	110
GDL porosity, ε_{GDL}	0.5
GDL permeability, K_{GDL} (m^2)	5×10^{-13}
MPL permeability (for $\varepsilon_{\text{MPL}} = 0.4$), K_{MPL} (m^2)	1×10^{-14}
Surface tension, liquid-water-air (80 $^\circ\text{C}$), σ (N/m)	0.0625
Oxygen diffusion coefficient in gas, D^{O_2} (m^2/s) [17]	1.805×10^{-5}
Liquid-water viscosity (80 $^\circ\text{C}$), μ_l (Pa s) [17]	3.43×10^{-4}
Liquid-water density (80 $^\circ\text{C}$), ρ_l (kg/m^3) [17]	974.85
Cathode gas viscosity (80 $^\circ\text{C}$), ν_g (m^2/s) [17]	20.59×10^{-6}
Cell temperature, T_{cell} ($^\circ\text{C}$)	80
Net water transport coefficient, α	0.5
Prandtl number for air [17]	0.6994
Schmidt number for air, ν_g/D^{O_2}	1.1407
Nusselt number for gas channel [17]	2.98

alyst layer to the channel, although it is small in magnitude compared to the production of water at the catalyst layer.

In Fig. 3, the oxygen concentration profiles predicted by UFT and M^2 models are compared. Here, the oxygen concentration in the channel is taken to be $10 \text{ mol}/\text{m}^3$, and the convective mass transport coefficient of oxygen in the channel (h_m) is calculated as $0.032 \text{ m}/\text{s}$ based on heat/mass transfer analogy [9]. In the UFT model, the gas-phase molecular diffusion is the only transport mode accounted for, therefore the sole effect of two-phase transport is the reduced effective diffusivity due to the reduced porosity for liquid flow. However, M^2 model further includes the convective transport by counter-flow of the gas phase and consequently, the oxygen concentration at the catalyst layer predicted by M^2 model is higher, even though the effective diffusivity of oxygen is less than the one calculated by UFT model, because of the higher liquid saturations predicted. The single

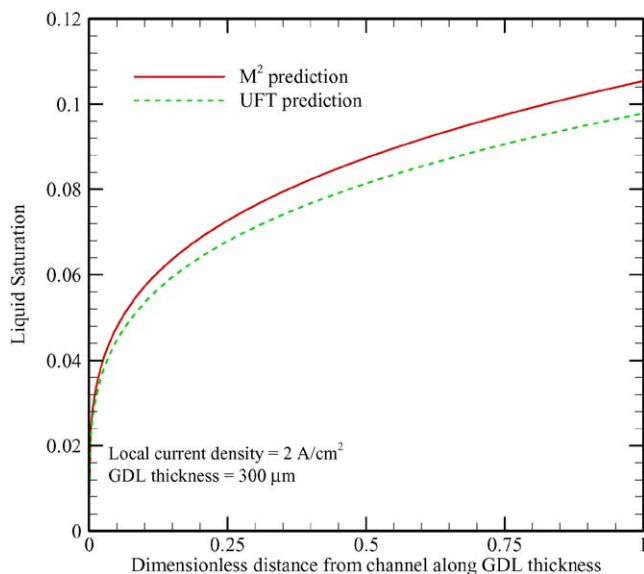


Fig. 2. Liquid saturation profile across the GDL.

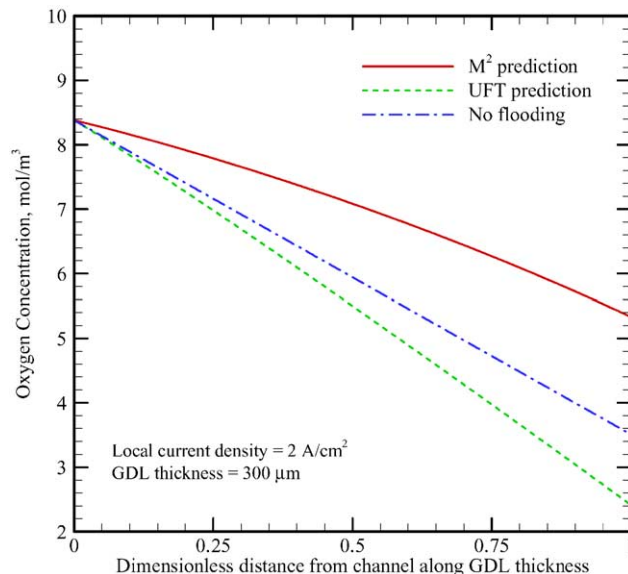


Fig. 3. Oxygen concentration profiles across the GDL.

gas-phase oxygen concentration profile in the GDL is also calculated and presented in Fig. 3 for comparison, which assumes that there is no effect of flooding on oxygen diffusion and naturally does not have the enhanced convection due to counter-gas flow. It is interesting to see that the two-phase transport in GDL enhances oxygen transport, due to the gas-flow counter to the capillarity-induced liquid flow. This enhanced oxygen transport effect is particularly dominant when the oxygen concentration is high in the gas channel. However, it should be noted that this oxygen transport enhancement exists only when the liquid saturation is low such that the reduced porosity for gaseous diffusion is not significant enough to offset the convective mechanism induced by the two-phase effect. In severely flooded GDL, the reduced gas-diffusion will dominate over the convection promoted by two-phase effects, and consequently a negative net effect on oxygen transport prevails.

In Fig. 4, the phase pressure profiles predicted by the two models are compared. The gas-phase pressure decreases across the GDL thickness in M^2 model predictions, whereas it is constant by definition in UFT model predictions. It is also clear from the same figure that M^2 model predicts a higher liquid pressure because of the counter-flow of the gas phase, which in turn causes higher liquid saturation.

3.2. Liquid-water transport in multi-layer diffusion media

Since MPL has significantly different material characteristics than GDL, the presence of an MPL may dramatically alter the two-phase transport and liquid saturation profile in the porous cathode of PEFC. As discussed in detail in the preceding sections, the difference in the characteristics of MPL and GDL causes a discontinuity in liquid saturation at the interface of the two layers. However, the magnitude of the discontinuity or the jump in the saturation is not only

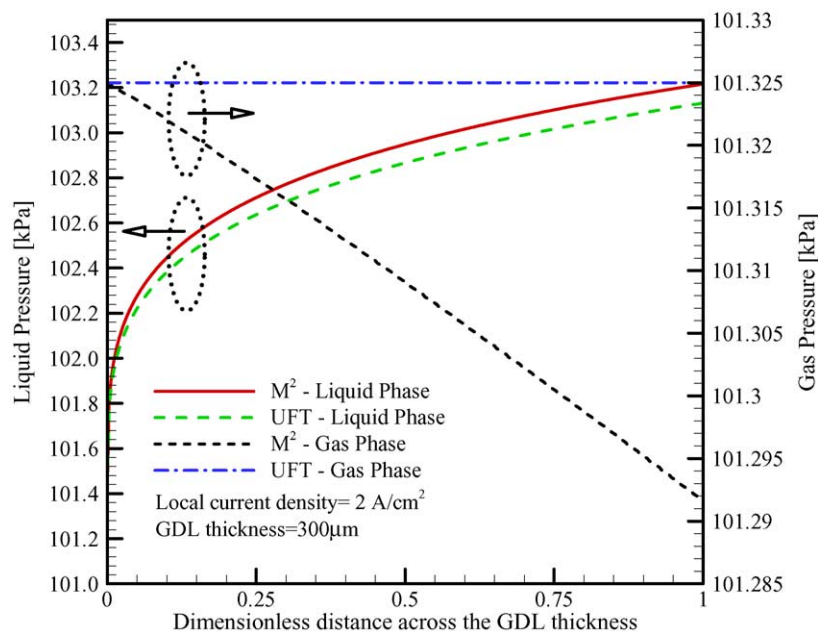


Fig. 4. Phase pressure profiles across the GDL.

dependent on the material properties of these two layers, but also on the liquid-water flux as suggested by Eq. (29). The discontinuity of saturation at the interface in multi-layer GDL can be utilized to enhance water transport and decrease the amount of liquid water in the MPL. However, it is essential to optimize the characteristics of these layers in order to utilize this advantage. Therefore, in this section, we analyze the effects of such parameters as the thickness, porosity and contact angle of the MPL.

MPL thickness: The MPL thickness plays an important role in the two-phase transport in the porous cathode. As seen in Fig. 5, the liquid saturation profile in MPL is greatly

affected by the thickness of MPL. Here, the total thickness of the cathode gas diffusion medium is kept constant at 300 μm. The liquid saturation in MPL is indeed lower at the MPL–GDL interface. However, as the thickness of MPL increases, due to the lower overall liquid permeability in MPL ($= k_{rl}K_{MPL}$), the liquid pressure across the MPL increases, which results in higher liquid saturation distribution in MPL. An MPL thickness of approximately 50 μm will cancel out the positive effect, rendering the liquid saturation at the GDL–catalyst layer interface nearly the same with or without the MPL.

In this work, we also compute the average liquid saturation in the cathode gas diffusion medium as a measure of the effectiveness of MPL, defined as:

$$s_{ave} = \frac{\int_0^{\delta_{GDL}} s_{GDL}(x) dx + \int_0^{\delta_{MPL}} s_{MPL}(x) dx}{\delta_{GDL} + \delta_{MPL}} \quad (35)$$

In Fig. 6, variation of this liquid saturation ratio with MPL thickness is shown. It is seen that the average liquid saturation in the cathode has a minimum when the thickness of MPL is between 30 and 45 μm. Although the catalyst layer liquid saturation is reduced further with the thinner MPL, the average liquid saturation increases with the thinner MPL due to higher contribution from the GDL liquid saturation. The liquid saturation at the catalyst layer–MPL interface is also plotted at the same figure, which clearly indicates that the catalyst layer saturation decreases with MPL thickness, as also seen from Fig. 5.

MPL porosity: The porous structure of both GDL and MPL is among the most important factors influencing the two-phase transport across the cathode. In this subsection, we analyze the effect of MPL porosity on the two-phase transport. Kozeny–Carman relation [16] is used to relate the

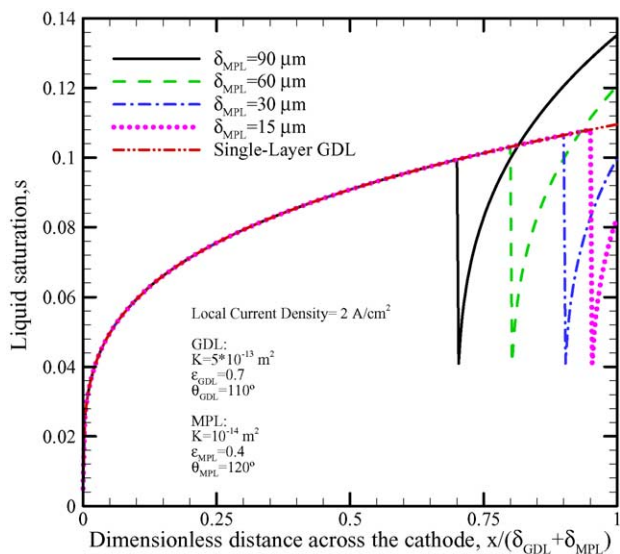


Fig. 5. Variation of liquid saturation in the multi-layer gas diffusion medium with micro-porous layer thickness.

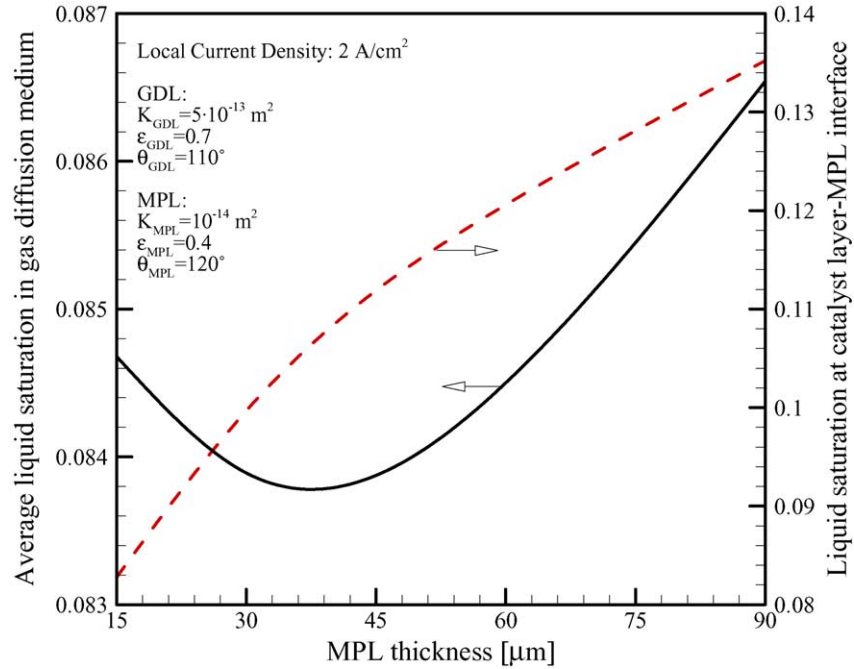


Fig. 6. Variation of the average liquid saturation in the multi-layer gas diffusion medium and liquid saturation at catalyst layer–MPL interface with MPL thickness.

porosity to the permeability of a porous medium and it is assumed that the pore diameters and Kozeny constant remain the same for different porosities of MPL. Kozeny–Carman relation is given by [16]:

$$K = \frac{\varepsilon^3 d^2}{16k_k(1 - \varepsilon)^2} \quad (36)$$

Since the pore diameter and Kozeny constant remain the same, it follows that:

$$\frac{K_1}{K_2} = \frac{\varepsilon_1^3(1 - \varepsilon_2)^2}{\varepsilon_2^3(1 - \varepsilon_1)^2} \quad (37)$$

In Fig. 7, the variation of liquid saturation profile with MPL porosity is shown. As seen from the inset of the figure, which shows the liquid saturation in the MPL at MPL–GDL interface versus MPL porosity, the jump in the saturation at the interface has a maximum around 0.6.

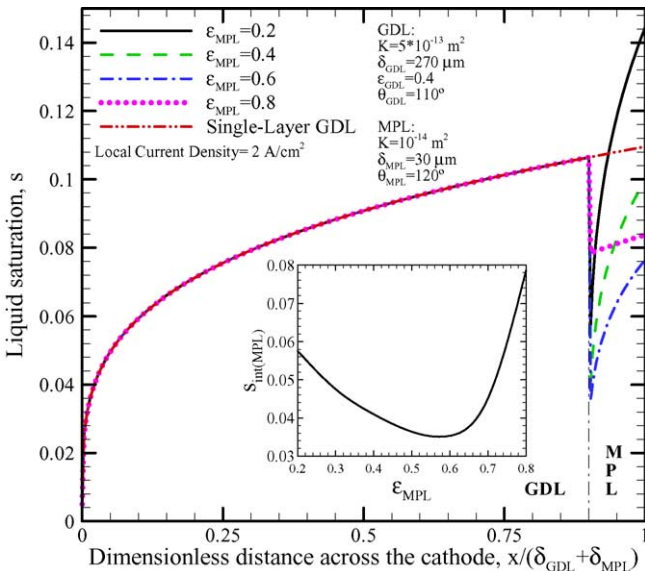


Fig. 7. Variation of liquid saturation in the multi-layer gas-diffusion medium with micro-porous layer porosity. The inset shows the variation of the liquid saturation in the MPL at MPL–GDL interface with MPL porosity.

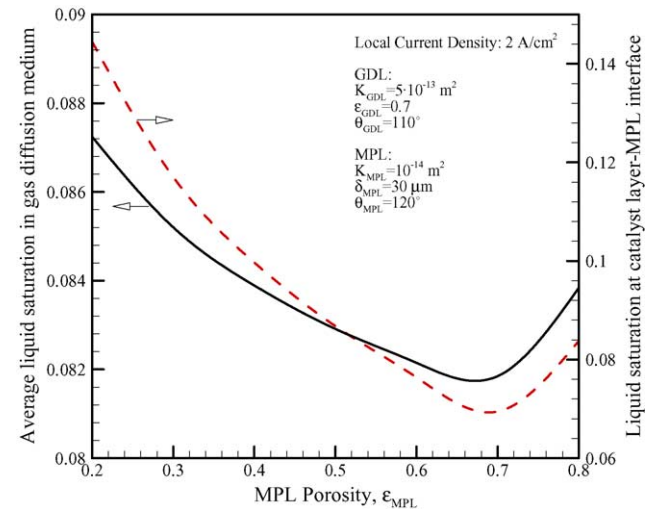


Fig. 8. Variation of the average liquid saturation in the multi-layer gas diffusion medium and liquid saturation at catalyst layer–MPL interface with MPL porosity.

Similarly, the average liquid saturation in the cathode gas diffusion medium and saturation at the catalyst layer–MPL interface have also a minimum around 0.7. With the higher porosity of MPL, the resistance to liquid-water flow in the MPL is smaller, therefore less pressure differential across the MPL is required. Consequently, the increase in the liquid saturation in MPL is smaller in larger porosities. This explains why while the maximum saturation discontinuity is seen around 0.6, the smallest liquid saturation at catalyst layer–MPL interface is seen around 0.7. With higher MPL porosity (e.g. 0.8), although the increase in liquid saturation in the MPL is smaller, the discontinuity is smaller; therefore catalyst layer saturation is actually higher (Fig. 8). However, with smaller MPL porosities, the discontinuity and the resistance to liquid-water flow is higher, resulting in higher liquid saturation in the MPL.

MPL wetting characteristics: As with the porosity, the contact angle of the MPL also affects the liquid transport and hence the liquid saturation profile. From Fig. 9, it is seen that, when the MPL contact angle is below a certain value, (around 95° for this case), the discontinuity at the MPL–GDL is reversed. Instead of lower saturation in MPL at the interface, the liquid saturation is higher in MPL and increases faster because of the weaker liquid-water transport due to the lower contact angle. It is clearly seen that with the increasing contact angle, the saturation discontinuity at the interface is enlarged and the increase in liquid saturation in MPL becomes smaller. This effect starts to disappear after a certain contact angle

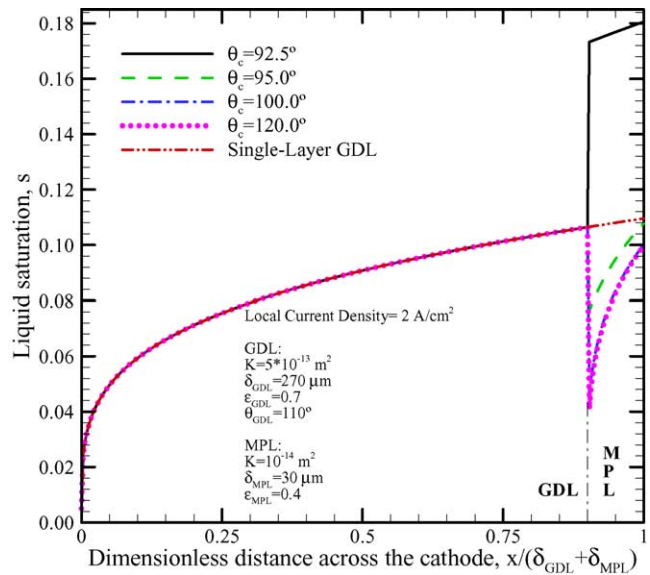


Fig. 9. Variation of liquid saturation in the multi-layer gas diffusion medium with MPL contact angle.

(around 105° for this case), since change in the MPL hydrophobicity ($\cos(\theta_c)$) becomes smaller. As also seen in Fig. 10, the average liquid saturation in the cathode gas diffusion medium decreases with the increasing contact angle, although the change in the average liquid saturation becomes much smaller with the higher MPL contact angles, similar to the catalyst layer–MPL interface saturation.

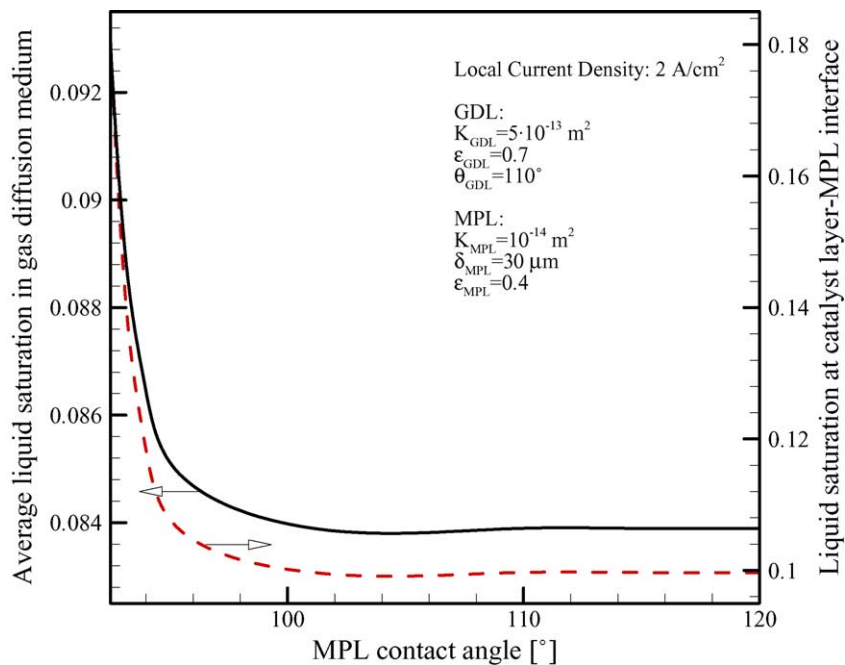


Fig. 10. Variation of the average liquid saturation in the multi-layer gas diffusion medium and liquid saturation at catalyst layer–MPL interface with MPL contact angle.

4. Conclusions

Two-phase transport in the porous layers of a PEFC cathode is investigated with the M^2 model and the following conclusions can be drawn from this study:

1. The effect of gas-phase pressure distribution in the GDL is found to an important factor, which is neglected by UFT model. Although the gas-phase pressure drop across the GDL is small (~ 30 Pa for a current density of 2 A/cm^2), the capillarity-driven counter-gas flow becomes an important factor, particularly in the low-saturation two-phase regime, since it enhances the transport of oxygen via convection and decreases the liquid pressure at the same capillary pressure. As a result, both oxygen concentration and liquid saturation profiles are affected. The effect of enhanced oxygen concentration is more pronounced at high oxygen concentrations (e.g. near the inlet or high pressure operation).
2. Placing a micro-porous layer between GDL and PEM enhances liquid-water removal and reduces the liquid saturation in the catalyst layer. From the analyses, it is seen that the catalyst layer liquid saturation is significantly decreased with use of a thin and highly hydrophobic micro-porous layer.

In this work, the analysis of MPL effect is limited to liquid-water transport in the cathode gas diffusion medium. However, due to significantly different micro-porous characteristics, MPL also affects the oxygen transport as well as electron transport in the cathode gas diffusion medium. Furthermore, MPL may affect the water transport across the membrane, since the hydraulic pressure balance across the membrane is altered by the presence of MPL. As an extension of this work, our efforts are underway to analyze these effects and further optimize the gas diffusion medium structure.

Acknowledgements

Funding for this work from Department of Energy under cooperative agreement no. DE-FC26-01NT41098, ConocoPhillips, GM Foundation, and NSF under Grant no. CTS-9733662 is gratefully acknowledged.

Appendix A. Nomenclature

C^i	molar concentration of species i (mol/m^3)
d	pore diameter (μm)
d_h	hydraulic diameter of the channel (m)
D_c	capillary diffusion coefficient (m^2/s)
D_h	hydraulic diameter (m)
D^i	diffusion coefficient of species i (m^2/s)
F	Faraday's constant (96,487 C/mol)
h_m	convective mass transfer coefficient (m/s)

I	current density (A/m^2)
\vec{j}_k	mass flux of phase k ($\text{kg/m}^2\text{s}$)
K	absolute permeability (m^2)
k	thermal conductivity (W/mK)
k_k	Kozeny constant
k_{rk}	relative permeability of phase k
mf_k^i	mass fraction of species i in phase k
M^i	molecular weight of species i (kg/mol)
Nu	Nusselt number ($= hd_h/k$)
p	pressure (Pa)
Pr	Prandtl number ($= \nu/\alpha$)
s	liquid saturation
Sc	Schmidt number ($= \nu/D^i$)
Sh	Sherwood number ($= h_m d_h/D^i$)
\vec{u}	velocity (m/s)

Greek letters

α	net water transport coefficient, thermal diffusivity ($k/\rho c_p$)
δ_i	thickness of layer i
ε	bulk porosity
γ_c	advection coefficient
λ_k	relative mobility of phase k
μ	dynamic viscosity (Pa s)
ν	kinematic viscosity (m^2/s)
θ_c	contact angle ($^\circ$)
ρ	density (kg/m^3)
σ	surface tension (N/m)

Subscripts

c	capillary
g	gas
int	interface
l	liquid
sat	saturation

Superscripts

GDL	gas diffusion layer
H_2O	water species
MPL	micro-porous layer
O_2	oxygen species

References

- [1] T.E. Springer, T.A. Zawodzinski, S. Gottesfeld, *J. Electrochem. Soc.* 138 (1991) 2334.
- [2] T.E. Springer, M.S. Wilson, S. Gottesfeld, *J. Electrochem. Soc.* 140 (1993) 3513.
- [3] T. Nguyen, R.E. White, *J. Electrochem. Soc.* 140 (1993) 2178.
- [4] W. He, J.S. Yi, T.V. Nguyen, *AIChE J.* 46 (2000) 2053.
- [5] Z.H. Wang, C.Y. Wang, K.S. Chen, *J. Power Sources* 94 (2001) 40.
- [6] L. You, H. Liu, *Int. J. Heat Mass Transfer* 45 (2002) 2277.
- [7] D. Natarajan, T.V. Nguyen, *J. Electrochem. Soc.* 148 (2001) A1324.
- [8] J.-H. Nam, M. Kaviany, *Int. J. Heat Mass Transfer* 46 (2003) 4595.
- [9] U. Pasaogullari, C.Y. Wang, *J. Electrochem. Soc.* 151 (2004) A399.

- [10] C.Y. Wang, in: W. Lietsich, A. Lamm, H.A. Gasteiger (Eds.), *Handbook of Fuel Cells—Fundamentals, Technology and Applications*, vol. 3, Wiley, Chichester, 2003.
- [11] C.Y. Wang, P. Cheng, *Adv. Heat Transfer* 30 (1997) 93.
- [12] U. Pasaogullari, C.Y. Wang, in: 203rd Electrochemical Society Meeting, 27 April–2 May 2003, Abstract Nr. 1190, Paris, France.
- [13] R.E. Meredith, C.W. Tobias, in: C.W. Tobias (Ed.), *Advances in Electrochemical Science and Engineering*, second ed., Interscience, New York, 1962.
- [14] C.S. Kong, D.Y. Kim, H.K. Lee, Y-G. Shul, T.H. Lee, *J. Power Sources* 108 (2002) 185.
- [15] Z. Qi, A. Kaufman, *J. Power Sources* 109 (2002) 38.
- [16] M. Kaviany, *Principles of Heat Transfer in Porous Media*, Springer, New York, 1999.
- [17] F.P. Incropera, D.P. DeWitt, *Fundamentals of Heat and Mass Transfer*, Wiley, New York, 1996.